29P

FINAL TECHNICAL REPORT FOR NAG 2-764

from

CALIFORNIA INSTITUTE OF TECHNOLOGY
Pasadena, California 91125

QUANTITATIVE UNDERSTANDING OF THE CYCLES OF OXIDIZED AND REDUCED SULFUR ON VENUS

Period Covered

March 1, 1992 through February 28, 1994

Yuk L. Yung, Principal Investigator
Professor of Planetary Science
Division of Geological and Planetary Science
California Institute of Technology
Pasadena, California 91125
818/395-6112

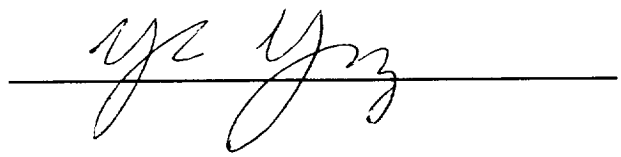

Introduction

The evolution of the Venus atmosphere is determined by the supply of gases from the interior of the planet and outer space, and by the loss of particles to space over time. In particular, questions pertaining to the initial inventory of water and the current and past rates of outgassing can be addressed by studying the loss rates of H, D, He_3 and He_4. The photochemistry of the H_2SO_4 clouds may also have played an important role in regulating the amount of water above the cloud tops, and hence limit the rate of escape of hydrogen from the planet. Thus the problems of evolution and chemistry are intimately related.

In our proposal the principal tasks we undertook to advance our understanding of the origin and evolution of water on Venus include:

(1) Escape of light atoms from Venus
(2) Photochemical model of sulfate formation

In the last two years we have made on Task (1) on how light atoms can escape from the exosphere of Venus with the development of a Monte Carlo program, and in Task 2 a thorough update on the SO_2 photochemistry has been carried out.

Task (1)

Escape Efficiencies of Light Species from the Venus Thermosphere

For nearly all escape mechanisms, particle mass becomes important. Hence, most escape mechanisms are more efficient for H than for D. In particular, charge exchange, currently the most important escape mechanism, has a D escape efficiency of only 2.6% relative to H escape, per individual particle. A second process, the subject of my work, is the ejection of light atoms (H, D, ^3He and ^4He) in collisions with fast moving oxygen-atoms. The atoms are the result of the energetic dissociative recombination of the O_2^+ ion in the ionosphere.

We have shown in past work that the efficiency of D escape relative to H escape for the collisional ejection process is about 60-70% per particle, whereas the process had initially been assumed to only allow for H escape. Our results lowered the escape flux of hydrogen by this process by about 65% to 3x10(6) cm^{-2} s^{-1} from the initial model of McElroy et al. (1982), relegating the process to a secondary role for overall hydrogen escape behind charge exchange. However, our finding of the strong efficiency of D escape showed that collisional ejection is the leading process for loss of deuterium, not charge exchange. The overall efficiency of both processes combined was revised upward from 1.3% to 12.5%, a nearly order of magnitude increase.

This efficiency is important in determining if a larger initial inventory of water was present that the 15 meter ocean discussed above. If, over the atmosphere's evolution, some D

is also escaping, this indicates that a proportionately larger amount of H (and therefore water) also escaped relatively to the 15 meter minimum.

Loss of atmosphere due to solar wind induced sputtering

Due to the lack of an intrinsic magnetic field, solar wind interacts directly with the exosphere of Venus. This can result in the acceleration of heavy ions (such as O^+) by the solar wind magnetic field. Sputtering by these accelerated ions has been identified as an important mechanism for the loss of atmosphere from Venus. The proper mathematical tool to handle this problem is the Monte Carlo technique.

We designed and implemented a Monte Carlo style model for determining loss rates due to solar wind induced sputtering from atmospheres. The model is general and can be applied to most atmospheres and contains many easily configured parameters. This allows atmospheres to be studied under various external conditions as well as allowing for evolution studies. Currently several different atmospheres have been implemented for Venus; both for testing and to look at the sputtering loss of light species. The detailed mechanics of this model will be briefly described in the following.

The sputtering model uses a Monte Carlo method to determine the sputtering efficiency of impacting O^+ ions. The sputtering efficiency is the number of ejected particles per incident particle. The model can be built using any atmosphere as long as it is sufficiently dense to stop the incoming particles and all the necessary information about the species in the atmosphere are included. This includes the atomic weight, cross--sections, scattering functions as well as the component atoms. For each run, the initial altitude, angle and energy can be chosen. The number of incident particles calculated can also be varied.

Any Monte Carlo method (there are many variations and many different ways of describing the process, but they are all very similar) is based on the statistics of large samples. For the sputtering problem, it is easiest to consider the Monte Carlo method as creating a virtual experiment and then analyzing the data. The model uses the model atmosphere and impacts ions on it. It uses pseudo-random numbers and the given probability distributions to determine where particles will impact and what happens during the impacts. It then traces the particles until they either "thermalize" or escape out the top of the atmosphere. It does this for a large number of impacting ions and then calculates the average escaping flux. A simple physical experiment to determine the escape rate would be to create the desired atmosphere and fire ions at it and see what comes out. Because it is impossible to actually perform this experiment, the Monte Carlo method is used perform the experiment instead. If the probability functions are good approximations of reality, the data from the method can be treated like data from the actual experiment.

The model operates by taking each initial particle and calculating its history in the atmosphere. For each initial particle, it calculates where its first collision will occur. It uses the same routine for calculating where any collision occurs. It uses the standard exponential distribution for collision path length. Once its chooses (using a pseudo random number) the

actual path length to the next collision, it goes through the atmosphere layer by layer until it finds the actual location of the collision (all locations are approximately referenced to the surface). The rest of the model keeps track of collisions instead of particles (the impacting species, location, and energy). The initial collision is put into a queue of collisions and each collision is processed until the queue is empty.

For each collision, the model first chooses the target species using the cross--sections and number densities. Next it determines the final energy and direction of each particle involved (there can be more than two if the target particle is polyatomic). This is done by randomly determining the final angles of sufficient particles to give the collision a unique solution and then calculating this solution. The model uses Newtonian physics to constrain the collision (although most are elastic, dissociation is treated inelastically). For each particle involved in the collision, the model then calculates the location of its next collision. At this point it checks to see if the particle has escaped or been thermalized. If it is a valid collision, it is added to the queue, otherwise it is just processed by statistic gathering routines.

Once the queue is empty, the model has calculated where all the energy for that impacting particle have gone. At this point, the results for that particle are calculated and processed. The model then takes the next initial ion and repeats the calculation. Once the desired number of initial particles have been run, the results are summarized and the mean sputtering efficiency for each species is calculated. The model also keeps track of other statistics and prints them out (number of collisions, energy distribution...).

The code is broken up into six different modules (currently the logical and physical modules correspond well). The first module is the atmosphere module and contains the atmosphere and other data about the constituents (some of the data is in other modules). The second module is the main module. It takes care of the initial setup and the queue of collisions. It also performs all the checking to see when particles escape or thermalize. The next module calculates collisions. It calculates the final energy and direction of each particle involved in a collision. The fourth module determines where collisions occur. It is takes a particle and its current location and figures out where its next collision will occur. The next model calculates the cross section of a given particle with all the species in the atmosphere. The final module is the statistics and printing module. It keeps track of all of the results and then prints them out at the end. The graphing part of the module is physically separate, but the rest of the module is currently in the main module.

The main module starts the model run by initializing all the necessary parameters and asking the user for the initial conditions desired. It next starts a loop where it runs the number of requested initial particles. Within the loop, it first initializes the initial particle and sets up the collision queue. Then it processes each collision in the queue by sending the information to the collision module. Within the collision module, the cross-section module is used to determine the actual cross-sections (the module uses table and several functions to determine them). Then it takes the cross-sections and determines the target species. With the target species it determines the number of final particles and uses the code for that type of

collision to determine results of the collision. After calculating the behavior of each particle after the collision, the depth module is used to determine where each next encounters a particle. The depth module first gets all the cross-sections from the appropriate module. Then it determines the collisional path length for the particle. Finally, it calculates where in the atmosphere the particle will have traveled through the appropriate path length. This is done by subtracting the path length of each layer until the layer with the collision is found. The remainder is then used to obtain the actual location. The data for each subsequent location is then returned from the collision module to the main routine. Back in the main routine, each collision is checked to see if the particle escaped or if the particle was thermalized. This information is given to the statistical module. Any valid collisions are added to the queue. Once the queue is empty, the main routine starts over with the next initial particle in the loop. Finally, when the desired number of particles have been run, the statistical and printing module is used to calculate the desired values and the results are printed out. The atmosphere module doesn't contain any code. It is referred to by the depth and collision modules.

Publications and Conference Presentations

Gurwell, M. and Yung, Y., 1993, Fractionation of hydrogen and deuterium on Venus due to collisional ejection, *Planet. Space Sci.*, **41**, 91-104.

Gurwell, M.A., Yung, Y.L., Kass, D., and Mills, F., Fractionation of hydrogen and deuterium on Venus due to collisional ejection. Presentation at the Recent Advances in Mars and Venus Atmospheric Research Session of the IAMAP/IAHS Conference held in Yokohama, Japan, July 1993.

Kass, D., and Yung, Y.L., 1994, Atmospheric Loss from Mars due to Solar Wind induced Sputtering, *Science*, in press.

Kass, D., and Yung, Y.L., 1993, Atmospheric Loss from Venus due to Solar Wind induced Sputtering, manuscript in preparation.

Task (2)

The published literature for sulfur chemistry has been critically reviewed for use in modeling the atmospheres of Venus and Io. We have compiled a new database for photon absorption by SO_2 and SO and have compiled a set of preferred rates for SO_x reactions.

1. SO_2 Photon Absorption

Our new database for SO_2 photon absorption started with the Manatt and Lane (1993) compilation. Their compilation over the wavelength range 1060 - 4030 Angstrom has wavelength resolution of ~ 1 Angstrom with uncertainty in the cross-sections of order 1% (due to the need to digitize published graphs) plus the original uncertainty for the measurements

they reviewed. We have retained the Manatt and Lane compilation for 1323 - 1969 Angstrom. For the wavelength range 1061 - 1322 Angstrom, we have selected the cross-section measurements by Suto, et al. (1982). Their measurements do not appear to suffer from the wavelength non-linearities present in the Golomb, et al. (1962), data selected by Manatt and Lane (1993) for this wavelength region. The Suto, et al. (1982), data have a wavelength resolution of 2 Angstrom and uncertainty of ±10 %. Their results have been digitized with an estimated accuracy of ~ 1-2 Angstrom for the digtiized wavelength and an estimated additional uncertainty of ~ 5 % for the digitized cross-section.

For the wavelength range of 1969 - 4060 Angstrom, we have selected three sets of measurements from the laboratory of J.A. Joens--Martinez and Joens (1992), Hearn and Joens (1991), and Sprague and Joens (1994). The Martinez and Joens (1992) data have a wavelength resolution of 1.0 Angstrom and uncertainty of ± 2 ~ 5 % in the cross-section for 1970 - 2400 Angstrom. The Hearn and Joens (1991) data have a wavelength resolution of 0.6 Angstrom and uncertainty of 4 % + 0.2e-20 cm2 molecule-1 for 2280 - 3390 Angstrom. The Sprague and Joens (1994) data have a wavelength resolution of 1.0 Angstrom and uncertainty of 1 % + 0.20e-22 cm2 molecule-1 for 3200 - 4050 Angstrom. All of these data were kindly provided in digital form by Prof. Joens--in advance of publication in the case of the Sprague and Joens (1994) results. With the assistance of new measurements by Joens this year (Joens 1994), we believe we have resolved the differences in wavelength calibration that existed between the Hearn and Joens (1991) and Martinez and Joens (1992) data. The difference in cross-section values between these two sets of data (after the 1994 wavelength re-calibration) are 2-3 times the mutual uncertainty in the overlap region. We are discussing resolution of this difference with Prof. Joens. The Hearn and Joens (1991) and Sprague and Joens (1994) data agree well in wavelength calibration and cross-section.

We have, also, extended our database to wavelengths shorter than those included in Manatt and Lane (1992). We have selected the recent measurements by Hamdy, et al. (1991) and by Cooper, et al. (1991ab). The Hamdy, et al. (1991), data have a wavelength resolution of 0.6 Angstrom and uncertainty of ±1 ~ 2 % for 147 - 1017 Angstrom. The Cooper, et al. (1991b), data have a wavelength resolution of 1 eV and uncertainty of ± 5 % for 77 - 2480 Angstrom. The Cooper, et al. (1991a), data have a wavelength resolution of 1 eV and uncertainty of ±10 % for 50 - 77 Angstrom. We have selected the Cooper, et al. (1991a), data for 50 - 77 Angstrom, the Cooper, et al. (1991b), data for 77 - 276 Angstrom, and the Hamdy, et al. (1991), data for 147 - 1017 Angstrom. The Hamdy, et al. (1991), and Cooper, et al. (1991b), data agree well over 147 - 276 Angstrom the overlap region and are consistent with the results obtained by Wu and Judge (1981). The Cooper, et al. (1991a), and Cooper, et al. (1991b), results agree well at 77 Angstrom.

Our database for the total absorption cross-section of SO_2 now extends from 50 - 4050 Angstrom with wavelength resolution 0.6 - 5 Angstrom and uncertainty of 1 - 15 %.

Two other major uncertainties related to SO_2 photochemistry are the neutral and ion

branching ratios. We could find no quantitative measurements of the neutral branching ratios for photo-dissociation of SO_2 so we have been forced to rely on qualitative observations provided by a number of researchers. Our quantum yields for the SO + O branch are 0.5 for shorter than 1130 Angstrom, 0.7 for 1130 - 1300 Angstrom, 0.95 for 1300 - 1650 Angstrom, greater than 0.99 for 1650 - 2101, and 1.0 for 2101 - 2203 Angstrom. Our quantum yields for the S + O_2 branch are 0.3 for shorter than 1300 Angstrom, 0.05 for 1300 - 1650 Angstrom, and less than 0.01 for 1650 - 2101 Angstrom. Our quantum yield for the S + O + O branch is 0.2 for shorter than 1130 Angstrom. Our estimate for the yields at 193 nm was recently confirmed by Felder (1994) based on unpublished results. Our estimated quantum yields are consistent with the qualitative observations provided by Watkins(1969), Lalo and Vermeil (1972), Welge (1974), Lalo and Vermeil (1974/5), Freedman, et al. (1979), Wilson, et al. (1982), Venkitachalam and Versohn (1984), Felder, et al. (1988), Effenhauser, et al. (1990), and Sato, et al. (1992). Our estimated uncertainty for the quantum yields is less than 50% for the SO + O branch, less than 100% for the S + O_2 branch, and less than 100% for the S + O + O branch. These neutral branching ratios differ significantly from those used for previous Io chemistry modeling (Summers 1985).

Photo-ionization branching ratios for SO_2 have been compiled from measurements by Cooper, et al. (1991a), Cooper, et al. (1991b), and Erickson and Ng (1981). The Cooper, et al. (1991ab), measurements have been discussed earlier. The Cooper, et al. (1991b), ionization branching ratio measurements and the Hamdy, et al. (1991), total ionization cross-section measurements were used to convert the photoionization efficiencies reported by Erickson and Ng (1981) into ionization branching ratios. The Erickson and Ng (1981) data have wavelength resolution of 1.4 Angstrom and were digitized and converted to ionization branching ratios with estimated accuracy of ~ 2 Angstrom and uncertainty of ~ 10 %.

2. SO Photon Absorption.

Our new database for SO photon absorption uses the measurements by Phillips (1981), Nee and Lee (1986), and Nishitani, et al. (1985). The Phillips (1981) data was measured with wavelength resolution of 0.82 Angstrom and uncertainty of 18 % for 1900 - 2320 Angstrom. A digitized version of the Phillips (1981) cross-sections was kindly provided by Manatt (1993) with digitized wavelength resolution of 1 Angstrom and digitization uncertainty of order 1 %. Per Phillips (1992), the digitized cross-sections have been multiplied by 0.88 to remove the unnecessary correction factor introduced by Phillips (1981). The digitized, corrected Phillips (1981) data has been used for 1901 - 2319 Angstrom. The Nee and Lee (1986) data was measured with wavelength resolution of 5 Angstrom and uncertainty of ± 60 % for 1150 - 1350 Angstrom. The Nee and Lee data was digitized with estimated wavelength accuracy of 5 Angstrom and uncertainty of less than 10 %. The Nee and Lee (1986) data has been used for 1158 - 1335 Angstrom. The estimated upper limit cross-section provided by Nee and Lee (1986) for 1350 - 1800 Angstrom has also been used. The Nishitani, et al. (1985), ionization efficiencies were measured with wavelength resolution of 2.3 Angstrom for 915 - 1206 Angstrom. The Nishitani, et al. (1985), data were digitized with estimated wavelength accuracy of 2.5 Angstrom and estimated uncertainty of less than 10 %.

These ionization efficiencies were converted into ionization partial cross-sections using the Nee and Lee (1986) data and by assuming the ionization quantum yield at less than 1159 Angstrom was 1.0. The Nishitani, et al. (1985), data has been used to determine the ionization quantum yield for 1159 - 1206 Angstrom and the total absorption cross-section for 915 - 1159 Angstrom.

We have found no measurements of SO photon absorption cross-sections at wavelengths shorter than 915 Angstrom. Consequently, we have chosen to adjust the tabulated cross-sections for O_2, Fennelly and Torr (1992), for use for SO at wavelengths shorter 915 Angstrom. The O_2 cross-sections were shifted by 179 Angstrom to longer wavelengths to account for the wavelength difference in the onset of ionization for O_2 and SO. The shifted O_2 cross-sections were then scaled to match in a least-square sense the scaled Nishitani, et al. (1985), results over 915 - 1206 Angstrom.

3. SOx Chemical Reactions

We have reviewed published compilations and measurements of chemical reaction rates involving SO_x compounds and have selected the rates we consider most accurate, as shown in Table 1.

References

Fennelly, J.A., and D.G. Torr, *Atomic Data and Nuclear Data Tables*, **51**, 321-363 (1992).

Nishitani, E., K. Fukuda, and K. Tanaka, *Bulletin of the Chemical Society of Japan*, **58**, 3475-3479 (1985).

Nee, J.B., and L.C. Lee, *Journal of Chemical Physics*, **84**, 5303-5307 (1986).

Colin, R., *Canadian Journal of Physics*, **47**, 979-993 (1969).

Dyke, J.M., L. Golob, N. Jonathan, A. Morris, M. Okuda, and D.J. Smith, 1818-1827 (1974).

Phillips, L.F., *Journal of Physical Chemistry*, **85**, 3994-4000 (1981).

Whyte, A.R., and L.F. Phillips, *Journal of Physical Chemistry*, **86**, 4327-4330 (1982).

Clerbaux, C., and R. Colin, *Journal of Molecular Spectroscopy*, **165**, 334-348 (1994).

Phillips, L.F., personal communication (1992).

Golomb, D., K. Watanabe, and F.F. Marmo, *Journal of Chemical Physics*, **36**, 958-960 (1962).

Watkins, I.W., *Journal of Molecular Spectroscopy*, **29**, 402-409 (1969).

Okabe, H., *Journal of the American Chemical Society*, **93**, 7095-7096 (1971).

Lalo, C., and C. Vermeil, Journal of Photochemistry 1, 321-325 (1972/3).

Hui, M-H., and S.A. Rice, *Chemical Physics Letters*, **17**, 474-478 (1972).

Welge, K.H., *Canadian Journal of Chemistry*, **52**, 1424-1435 (1974).

Lalo, C., and C. Vermeil, *Journal of Photochemistry*, **3**, 441-454 (1974/5).

Freedman, A., S-C. Yang, and R. Bersohn, *Journal of Physical Chemistry*, **70**, 5313-5314 (1979).

Wu, C.Y.R., and D.L. Judge, *Journal of Chemical Physics*, **74**, 3804-3806 (1981).

Vasudev, R., and W.M. McClain, *Journal of Molecular Spectroscopy*, **89**, 125-133 (1981).

Erickson, J., and C.Y. Ng, *Journal of Chemical Physics*, **75**, 1650-1657 (1981).

Wu, C.Y.R., and D.L. Judge, *Geophysical Research Letters*, **8**, 769-771 (1981).

Wilson, M.W., M. Rothschild, D.F. Muller, and C.K. Rhodes, *Journal of Chemical Physics*, **77**, 1837-1841 (1982).

Suto, M., R.L. Day, and L.C. Lee, *Journal of Physics B: Atomic and Molecular Physics*, **15**, 4165-4174 (1982).

Kawasaki, M., K. Kasatani, and H. Sato, *Chemical Physics*, **73**, 377-382 (1982).

Wu, C.Y.R., *Journal of Physics B: Atomic and Molecular Physics*, **17**, 405-416 (1984).

Venkitachalam, T., and R. Bersohn, *Journal of Photochemistry*, **26**, 65-67 (1984).

Gallagher, et al., *Journal of Physics and Chemistry Reference Data*, **17**, 128-129 (1988).

Ebata, T., O. Nakazawa, and M. Ito, *Chemical Physics Letters*, **143**, 31-37 (1988).

Felder, P., C.S. Effenhauser, B.M. Haas, and J.R. Huber, *Chemical Physics Letters* **148**, 417-422 (1988).

Effenhauser, C.S., P. Felde, and J.R. Huber, *Chemical Physics*, **142**, 311-320 (1990).

Felder, P., personal communication (1994).

Joens, J.A., personal communication (1994).

Hearn, C.H., and J.A. Joens, *Journal of Quantitative Spectroscopy and Radiative Transfer* **45**, 69-75 (1991).

Cooper, G., E.B. Zarate, R.K. Jones, and C.E. Brion, *Chemical Physics* **150**, 251-261 (1991a).

Cooper, G., E.B. Zarate, R.K. Jones, and C.E. Brion, *Chemical Physics*, **150**, 237-250 (1991b).

Hamdy, H., Z.X. He, and J.A.R. Samson, *Journal of Physics B: Atomic and Molecular Optical Physics* **24**, 4803-4807 (1991).

Ahmed, S.M., and V. Kumar, *Journal of Quantitative Spectroscopy and Radiative Transfer*, **47**, 359-373 (1992).

Martinez, R.D., and J.A. Joens, *Geophysical Research Letters*, **19**, 277-279 (1992).

Sato, T., T. Kinugawa, T. Arikawa, and M. Kawasaki, *Chemical Physics*, **165**, 173-182 (1992).

Manatt, S.L., and A.L. Lane, *Journal of Quantitative Spectroscopy and Radiative Transfer* **50**, 267-276 (1993).

Mitsuke, K., S. Suzuki, T. Imamura, and I. Koyano, *Organic Mass Spectrometry* **28**, 335-339 (1993).

Sprague, K.E., and J.A. Joens, submitted for publication (1994).

Manatt, S.L., (1993).

TABLE 1

Photodissociation Reactions (calculated at Jupiter's mean distance from the Sun and zero optical depth for solar minimum)

	Summers		Mills
O2 + hv -> 2O	9.1(-8)		
SO + hv -> S + O	1.1(-5)		
SO2 + hv -> SO + O	2.8(-6)		7(-8)
SO2 + hv -> S + O2	1.0(-6)	y4 = 0.5	2(-7)
S2 + hv -> 2S	5.2(-5)		

neutral + neutral reactions

Reaction	Summers A	Summers B	DeMore (JPL, 1992) A	DeMore (JPL, 1992) B	Least-Squares Fit to NIST A	Least-Squares Fit to NIST B	Least-Squares Fit to NIST C	Atkinson et al. (1992) A	Atkinson et al. (1992) B	Atkinson et al. (1992) C	Recommendation A	Recommendation B	Recommendation C
(assumed temperature range for reactions is 100 - 600 K, DeMore's values are for 200 - 300 K)													
Two-body Reactions (sulfur and oxygen):													
S + SO -> S2 + O	not included		not included		1.0(-12)	-11500	0.50#	not included			1.0(-12)	-11500	0.50#
S + O -> SO + hv	not included		not included		not included			not included			5.98(-24)	+1.58**	
											{assumed same as O + O}		
S + O2 -> SO + O	2.3(-12)	0	2.3±1.2(-12)	0±200	2.3(-12)	-7.2		2.1(-12)			2.2(-12)		
								2.3(-12) {Millar et al 1991}					
S + O3 -> SO + O2	1.2(-11)	0	1.2±2.0(-11)		1.2(-11)	(298 K only)		1.2(-11)			1.2(-11)		
SO + SO -> SO2 + S	5.8(-12)	-1760	not included		4.2(-15)	(298 K only)		<1.7(-14)			4.2(-15)		
								{Baulch et al 1976}					
SO + (SO)2 -> SO2 + S2O	not included		not included		not included			not included			3.3(-14)		
								3.3(-14) {Herron & Huie 1980}					
SO + SO3 -> 2SO2	2.0(-15)	0	not included		2.0(-15)	(298 K only)		not included			2.0(-15)		
SO + O -> S + O2	not included		not included		not included			6.60(-13)	-2760		6.60(-13)	-2760	
								{Millar et al 1991}					
SO + O -> SO2 + hv	not included		not included		not included			3.20(-16)	-1.50@		1.66(-12)	-1.50**	
								{Millar et al 1991}					
SO + O2 -> SO2 + O	2.4(-13)	-2370	2.6±2.0(-13)	-2400±500	1.6(-13)	-2300		1.4(-13)	-2280		1.6(-13)	-2300	
								1.40(-12)	-2820				
								{Millar et al 1991}					
SO + O3 -> SO2 + O2	2.5(-12)	-1100	3.6±1.2(-12)	-1100±200	4.1(-12)	-1140		4.5(-12)	-1170		4.1(-12)	-1140	
SO2 + O -> O2 + SO	not included		not included		8.3(-12)	-9800		2.08(-10)	-9980	-0.511#	8.3(-12)	-9800	
								{Baulch et al 1976}					
								1.30(-9)	-9140	-0.46#			
								{Millar et al 1991}					
SO2 + O3 -> SO3 + O2	not included		3.0(-12)	<-7000	1.4(-12)	-7000		not included			3.0(-12)	-7000	

S2 + O -> SO + S	not included	not included	not included	6.6(-12) {Baulch et al 1976} 1.73(-11) 0.50@ {Millar et al 1991}	6.6(-12)
O + O -> O2 + hv	not included	not included	not included	4.90(-20) +1.58@ {Millar et al 1991}	5.98(-24) +1.58**
O + O3 -> 2O2	1.5(-11) -2218	8.0±1.15(-12) -2060±250	1.2(-11) -2140	8.0(-12) -2060	8.0(-12) -2060

Two-body Reactions (sodium):

Na + O3 -> NaO + O2	not included	7.3(-10) 0±200	6.0(-10) -195	1.05±0.12(-9) -116±26.0 {Plane et al 1993}	1.1(-9) -116
Na + O3 -> NaO2 + O	not included	<4.0(-11) (298K only)	only old JPL value included	6.0±1.2(-10) (T/200)^0.5 {Plane 1991}	<4.0(-11)
Na2O + O -> 2NaO	2.0(-11) 0	not included	not included	not included	2.0(-11)
NaO + O -> Na + O2	1.6(-10) 0	3.7±3.0(-10) 0±400	3.7(-10) ###	2.2±0.5(-10) (T/200)^0.5 {Plane & Husain 1986}	3.7(-10)
NaO + O3 -> NaO2 + O2	not included	1.6±2.0(-10) 0±400	not included	1.11±0.34(-9) -567.7±69.8 {Plane et al 1993}	1.1(-9) -570
NaO + O3 -> Na + 2O2	not included	6.0±3.0(-11) 0±800	not included	3.2(-10) -550 {Plane et al 1993}	3.2(-10) -550
NaO2 + O -> NaO + O2	2.5(-11) 0	not included	not included	not included	5±2(-10) -940±180 {Helmer & Plane 1993}

other sodium and oxygen compound reactions listed in Helmer and Plane 1993 and Plane 1991
other sodium and sulfur compound reactions listed in Schofield and Steinberg 1992

Three-body Reactions:***

S + O + M -> SO + M	not included	not included	not included	not included	9.6(-32) +460 -0.89# {assumed same as O + O + M}
2S + M -> S2 + M	2.0(-33) 0	not included	1.2±0.17(-29) (295 K only) {Nicholas et al 1979}	2.8(-33)-1.2(-29) {Baulch et al 1976}	1.2(-29)
2S2 + M -> S4 + M	not included	not included	not included	1.7(-33) +1700 {Baulch et al 1976}	1.7(-33) +1700
SO + SO + M -> (SO)2 + M	not included	not included	4.4(-31) 0 {Herron & Huie 1980}	"only important at high T" ~1(-33) {Cobos et al 1985}	1(-33)
SO + O + M -> SO2 + M	6.0(-31) 0	not included	6.7(-27) -1.6**	1.8(-31)	6.7(-27) -1.6**
SO2 + O + M -> SO3 + M	8.0(-32) -1000	not included	3.9(-32) -1020	4.0(-32) -1000	4.0(-32) -1000
2O + M -> O2 + M	8.6(-28) -2 **	not included	9.6(-32) +460 -0.89#	5.2(-35) +900 {Baulch et al 1976}	9.6(-32) +460 -0.89#
O2 + O + M -> O3 + M	1.35(-33) 0	6.0±0.5(-34) -2.3±0.5@	1.5(-30) +166 -1.5#	6.0(-34) -2.8@	5.2(-27) -2.8**
Na + O + M -> NaO + M	1.0(-33) 0	not included	not included	not included	1.0(-33)

Na + O2 + M -> NaO2 + M	8.4(-34)	+/-290?	2.4±0.5(-30)	-1.2±0.5##	9.3(-27)	-1.46**	3.06±0.34(-30)	-1.30±0.04@	5.1(-27)	-1.30**	T>240K
			4.0±2.0(-10)	0±1.0			5.0(-30) (T/200)^-1.22		3.2(-27)	-1.22**	T<240K
			low pressure limit equivalent to		2.3(-27)	-1.2**					
NaO + O2 +N2 -> NaO3+N2	not included		3.5±0.7(-30)	-2.0±2.0##	1.1(-25)	-2			3.2(-25)	-2.0**	
			5.7±3.0(-10)	0±1.0							
			low pressure limit equivalent to		3.2(-25)	-2.0**					

Notes:

means rate constant follows form A * exp(B/T) * (T^C)
@ means rate constant follows form A * ((T/300)^B)
** means rate constant follows a power law form: A * (T ^ B)
means rate constant follows form in DeMore (1992)
all other rate constants follow an Arrhenius form: A * exp(B / T)

*** all three body reaction rates derived from NIST information are for the low pressure limit
value selected by DeMore et al for 200-300 K is same as measured value for 573 K so no known temperature dependence

Uncertainties are included for DeMore's values. No uncertainties included for Summers', NIST, or mine.
How to calculate DeMore's uncertainties:

f(T) = f(298) * exp(abs((delta-E/R) * ((1/T)-(1/298))))
where f(298) is the uncertainty in A given in the table above
delta-E is the uncertainty in B given in the table above
the exponent is absolute value

units for two-body reaction constants (A) are cm3 molecule-1 second-1
units for three-body reaction constants (A) are cm6 molecule-2 second-1

This paper (which has been accepted by *Science* is Part I of two papers based on the same technique. Part II (on Venus) is in preparation.

Atmospheric Loss from Mars due to Solar Wind Induced Sputtering

D. M. Kass* and Y. L. Yung[1]

Abstract. Since Mars does not have a strong intrinsic magnetic field, the atmosphere is eroded by interactions with the solar wind. Luhmann *et al.* (1) showed that early solar system conditions favor sputtering. Using a new sputtering model we calculate that ~2.3 bars of CO_2 have been lost over the last 3.5 billion years. This significant increase over the previous estimate of ~0.14 bar of CO_2 lost through sputtering (1) is due to a more complete model. During the same time, the escape of O by all methods removed ~60 m of water (a slight increase over the previous estimate of ~50 m (1)). Since estimates of CO_2 on early Mars range from 0.5 to 5 bars of CO_2 (2,4), a loss of 2 bars is significant whereas the previous estimate of 0.14 bar was rather insignificant. This new value will help solve the problem of what happened to the initial Martian atmosphere and probably have a large impact on our understanding of the evolution of early Mars.

[1] Division of Geological and Planetary Sciences, California Institute of Technology, Pasadena CA 91125.

Martian geomorphology, notably the channels, appears to indicate that the planet once had significant quantities of water at or near the surface and a much higher surface temperature, possibly caused by an atmospheric greenhouse. While there are questions about how much a greenhouse could raise the temperature (3), all current models require an atmosphere of at least half a bar of CO_2 to have liquid water (2,4). Since the current Martian atmosphere has only 7mbar of CO_2 and only a small amount of H_2O, an important question is the fate of the early water and CO_2.

There are two major possibilities: either the early atmosphere is sequestered somewhere in the planet (4) or it has been lost to space. None of the common escape mechanisms, such as Jeans escape or solar wind pickup, is capable of removing significant amounts of CO_2 or water over the lifetime of the planet. Luhmann *et al.* (1,5) proposed that atmospheric sputtering by O^+ could account for the loss of a significant amount of water, but could not account for the CO_2 loss. In this process, hot ions (notably O^+) are accelerated out of the ionosphere by the interaction of the solar wind and interplanetary magnetic field with the upper atmosphere. These ions follow helical trajectories and often reimpact the atmosphere with significant amounts of energy (upwards of 1 keV). During the impact, they can, through collisions, accelerate and cause other particles to escape.(5)

Luhmann *et al.* (1) used a model to calculate the sputtering loss of CO_2 and water from Mars over the last 3.5 Gyr. They calculated the escaping flux at three epochs (3.5 Gyr ago, 2.5Gyr ago and the present) referred to as 6 EUV, 3 EUV and 1 EUV respectively (6). At each epoch they first calculated the flux of reimpacting O^+ ions (7). Then they used an analytic

model (8) to calculate the efficiency (number of particles ejected per incident particle) of the carbon and oxygen. These were used to calculate total fluxes integrated over the planet. By assuming that the C and O come from CO_2 and H_2O (and adding in other escape fluxes of O), the loss rate of CO_2 and H_2O can be calculated at each epoch. These rates are then integrated from 3.5 Gyr ago to the present. Luhmann *et al.* (1) found that ~0.14 bars of CO_2 and ~50 m of water have been lost. While this is sufficient water to form the erosional features, it is only a fraction of the necessary CO_2.

Luhmann *et al.* (1) appear to have neglected several factors in their model. The first is that they treat CO_2 as atomic components, but when a CO_2 molecule is involved in a collision, all components are affected and thus the C effectively has the cross--section of the whole molecule. They also did not fully account for secondary collisional ejections. These are particles ejected by secondary particles that were accelerated by the impacting ion and still had sufficient energy to accelerate other particles to escape. The first effect specifically increases the C escape efficiency whereas the second one results in an increase in the escape efficiency of all species.

We used a general Monte--Carlo type atmospheric sputtering model (9) adapted for Mars. The initial conditions were chosen to match those of Luhmann *et al.* (1,5). Apart from the polyatomic dissociation (10), the model uses elastic collisions with anisotropic scattering functions (11). Many of the cross--sections used in the calculation are the hard sphere geometric cross--section, but where they exist, more realistic energy dependent ones were used.

For modern Mars, an atmosphere from Nair *et al.* (12) ranging from 50 up to 240 km was extrapolated hydrostatically up to 450 km. The model contains the seven most common species

on Mars at these altitudes (CO_2, CO, O, H_2, N_2, N, H). The ancient atmospheres of 3.5 and 2.5 Gyr ago were taken from Luhmann *et al.* (1). They modeled only the two major species (O and CO_2) between 150 and 300 km. Both atmospheres were extrapolated to cover the range from 125 up to 450 km.

Our basic model was compared to the results in Luhmann and Kozyra (5) for both Venus and Mars. When the model was modified to reflect the assumptions of their two stream model (see Table 1), the results agreed to within 30%. This is a reasonable difference given the coarseness and uncertainties of both models. The analytic models of Johnson (8) also have similar accuracies and match our model results to within 20%. Using these comparisons and considering the number of poorly constrained parameters, the model is probably accurate to within 50% (13).

The model was used to calculate the escape efficiency for C and O at each epoch (results in Table 1). The total efficiency (the number of atoms, regardless of species) does not vary much because it is primarily controlled by the escape energy which only depends on gravity. While the total number of atoms is fairly constant, the relative fraction of each species is controlled by the composition of the atmosphere around the exobase. The precipitating O^+ generally has its first collision near the exobase (due to the definition of the exobase). The exponential increase in density of the atmosphere results in a rapid decrease in the collisional path length below this point and causes most of the subsequent collisions to occur within a relatively narrow altitude band around the exobase. Thus the relative abundance of the atmospheric constituents in this area affects the relative escape efficiencies.

Since the relative abundance of CO_2 at the exobase increases with time, the increase of the C:O escape efficiency ratio is expected. The C:O ratio is around 1:2 since CO_2 is the dominant species. The deviation is due to the presence of other species in the atmosphere, especially atomic O and CO. Also, since it is lighter, the C is preferentially lost from the CO_2. The slight excess of C (compared to 1:2 ratio expected from CO_2) escaping at present is more than balanced by the O fluxes due to other escape mechanisms.

The results indicate that the two effects neglected by Luhmann *et al.* (1) in their analytic model are important on Mars. By dissociating the CO_2 only during a collision, our model increases the C escape efficiency by a factor of 2. While the cross--sections of CO_2 is closer to three times that of atomic C, this is reduced by the collision energy being divided among all three particles and by the energy used to dissociate CO_2. The effect of the multi-species, multi-collision sputtering increases the efficiency on Mars by almost an order of magnitude, because previously "thermalized" particles still had sufficient energy to excite others collisionally and cause them to escape.

The model efficiencies for each epoch were multiplied by the precipitating O^+ fluxes calculated by Luhmann *et al.* (1,6) to obtain the actual escaping fluxes (Table 2). As can be seen from Figure 1, all fluxes have decreased with time. This is especially true for the sputtered species--even for CO_2, whose efficiency increases with time. The closer it is to the present, the weaker are the EUV and solar wind and thus the smaller is the precipitating flux. The large decrease in precipitation overwhelms any small increases in efficiency.

In order to calculate the total fluxes, each C atom is assumed to come from a CO_2

molecule whose O atoms escape separately. The escaping O that cannot be part of a CO_2 molecule (constrained by the C flux) is reported as the H_2O flux. It contains not only the O lost through sputtering, but also the O lost by the other major mechanisms. Photochemistry of the Martian atmosphere indicates that this O effectively comes from H_2O (12).

When these planetary loss rates are integrated over the last 3.5 Gyr the total CO_2 and H_2O lost since the current atmosphere formed can be calculated. This yields losses of 1.2×10^{44} molecules of CO_2 and 3×10^{44} molecules of H_2O. The sputtered CO_2 represents ~2.3 bars, and the H_2O is equivalent to ~60 m of water.

The integrated fluxes are important for our understanding of the history of the Martian atmosphere and surface. Certain features, notably channels, seen on Mars have been interpreted as erosional features due to liquid water on or near the surface. There has been a lot of modeling of possible early atmospheres and surface conditions of Mars to consider how they could have been formed. There are two important parameters: mean surface temperature and volume of water. The problem is that the models indicate that at least 50 m of water (14) and 0.5 bars of CO_2 (15) are needed to create the features. While CO_2 cannot raise the surface temperature to 273K (3), sufficient heating could be created with as little as 0.5 bars (for ice covered lakes (15)), and around one bar meets the requirements of most models. Until now, the problem has been determining where this water and CO_2 went. With our current modeling results, this is no longer a problem: all of the water and CO_2 could have been lost to space by sputtering (and other escape mechanisms) over the age of the planet.

Since most of the major sputtering occurred early in the history of Mars, it is difficult to

test the model results. Actual measurements of the modern escape fluxes of heavier species from Mars would help constrain at least the value for the present epoch and verify the validity of the sputtering model itself. This is especially the case for C since sputtering appears to be the dominant escape mechanism (for O, the other escape mechanisms will overwhelm the contribution from sputtering). Atmospheric stable isotope data may also help constrain the total amount lost from the atmospheric reservoir, but there appear to be large uncertainties in the interpretation of the data (16). The best method to constrain the early atmosphere is probably in situ geochemical and geological measurements at Mars.(17)

Notes

1. Luhmann, J. G., R. E. Johnson, M. H. G. Zhang, *Geophys. Res. Lett.*, **19**, 2151 (1992).

2. Hunten, Donald M., *Science*, **259**, 915, (1993). Jakosky, Bruce M., *Icarus*, **94**, 14 (1991). Kasting, James F., *Icarus*, **94**, 1, (1991). Kieffer, H. H., B. M. Jakosky, C. W. Snyder, M. S. Matthews, Eds., *Mars* (Univ. of Arizona Press, Tuscon, 1992). McKay, Christopher P. and Wanda L. Davis, *Icarus*, **90**, 214 (1991). Pollack, J. B., J. F. Kasting, S. M. Richardson, and K. Poliakoff, *Icarus*, **71**, 203 (1987).

3. Kasting, James F., *Icarus*, **94**, 1, (1991).

4. Fanale, F. P., J. R. Salvail, W. B. Bandert, and R. S. Saunders, *Icarus*, **50**, 381 (1982).

5 Luhmann J. G. and J. U. Kozyra, *J. Geophys. Res.*, **96**, 5457 (1991).

6. Sputtering fluxes are affected by three main parameters: the atmosphere, the solar wind and the extreme ultra--violet (EUV) solar emission. All three parameters have changed over the history of the solar system. The earlier atmosphere was much denser, but the major effect on sputtering is the changing CO_2 to O ratio at the exobase. The early solar wind was much stronger (both the velocity and the interplanetary magnetic field) and thus increased the amount of energy an ion gained before impacting. While the "young sun" is thought to have been faint in the visible, it was much more active in the EUV. The enhanced EUV would create more ions and thus enhance the impacting flux. At 2.5 Gyr ago, the EUV flux was three times the current value and at 3.5 Gyr ago, it was six times the current value (this is for the entire EUV, the ionizing radiation may have been as high as 100 times the current flux). Thus the names 6 EUV, 3 EUV and 1 EUV used for the three epochs.

7. The impact flux was calculated by Luhmann *et al.* (1,5) by first using a gas-dynamic solar wind interaction model and the upstream parameters for the sun at the appropriate age to calculate the magnetic and electric fields around Mars. Then test particles are launched from a grid over the planet and the trajectory of each one is calculated by numerical integration. If the particle impacts the planet, it is counted, weighted by the ion density of its source region. These values are then summed to give effective impacting fluxes of 4.8 x 10^5 (1 EUV), 1.6 x 10^8 (3 EUV), 2.6 x 10^9 (6 EUV) particles s^{-1} cm^{-2} normalized to 1 keV particles.

8. Johnson, R. E., *Energetic Charged-Particle Interactions with Atmospheres and Surfaces*, (Springer--Verlang, New York, 1990). The model assumes that the atmosphere is composed of the appropriate number densities of atomic constituents (based on the number densities of the various actual species) at the exobase. This is then treated as a "solid" surface and the analytic sputtering formulas for solid surfaces are applied after being modified for the given situation.

9. In the Monte--Carlo model, the effect of individual impacting particles are calculated. These are then averaged over a large number of impactors (5000 in most cases) to determine the average effect. For a particle, the code determines randomly (using an exponential functional form) where the next collision happens. It uses the cross--sections to determine randomly what it collides with. The result of the collision is then determined with the scattering angle randomly determined with the appropriate functional form. Each particle resulting from the collision is tracked. Particles keep colliding until they thermalize or escape. Once all the products of one incident particle have been tracked, the next one is calculated. The model implementation was tested by setting the parameters to create simple cases that can be analyzed analytically and by

comparison to simpler models.

10. Due to the high energy of the impacting particles (initially ~1 keV), whenever a polyatomic particle is involved in a collision, it will dissociate completely (and thus "absorb" the binding energy). The molecules only dissociate if the impacting particle has sufficient energy to dissociate the target and allow its fragments to escape.

11. Due to the lack of data on the scattering functions, most of them were modeled using a Henyey--Greenstein function with a g value of 0.5 for neutral collisions and 0.9 for ions (reflecting the tendency to only charge exchange in the ion collisions). For a couple cases where there is some data, double Henyey--Greenstein functions were used. The model is fairly insensitive to the actual shape of the functions over a range of reasonable g values.

12. Nair, Hari, Mark Allen, Ariel D. Anbar, Yuk L. Yung, and R. Todd Clancy, *Icarus*, 1994, in press.

13. This is only the error for the Monte-Carlo model and ignores any uncertainty in the calculation of the precipitating O^+ flux. There are three main sources of uncertainty in the model. The first one has to do with the cross--sections and scattering functions. Very few of these have been measured or calculated quantum mechanically. While the model is fairly insensitive to the individual values, there are so many that are poorly constrained that the overall effect is considerable. The second source of error is the atmosphere models. This is especially the case for the ancient atmospheres. The third major uncertainty is in normalizing the impacting flux. There is also some uncertainty introduced by the numerical modeling, but it is minor compared to the sources mentioned above.

14. Baker, V. R., M. H. Carr, V. C. Gulick, C. R. Williams, and M. S. Marley, *Mars* (Univ. of Arizona Press, Tuscon, 1992) chap. 15.

15. McKay, Christopher P. and Wanda L. Davis, *Icarus*, **90**, 214 (1991).

16. Jakosky, Bruce M., *Icarus*, **94**, 14 (1991). He indicates that for loss from the exobase, there would have to be an equal amount of atmosphere buried in the planet. Preliminary calculations for C^{13} indicate that anywhere from 1 to 5 bars of CO_2 need to be buried to match the δC^{13} atmospheric measurements.

17. DK was supported by an NSF Fellowship and this work was partly supported by NASA grant NAGW--1538 and NAG 2--764.

Table 1. Sputtering efficiency per incident O^+ calculated by the model for 3 epochs. The values for the current work are the complete model with dissociation and full accounting of all secondary particles. The "simplified" model is a modification of the full model that implements the assumptions of Luhmann and Kozyra (5). The assumptions of the "simplified"' model insure that no C will be sputtered. All of the efficiencies are in atoms per impacting 1 keV O^+.

	Epoch		
	6 EUV (1 Gyr)	3 EUV (2 Gyr)	1 EUV (4.5 Gyr)
Current Work			
O:	11.8	11.2	9.96
C:	3.29	4.23	5.47
Simplified			
O:	1.70	1.25	0.65
C:	0.00	0.00	0.00

Table 2. Net escape fluxes from Mars for 3 epochs. Each flux is integrated over the disk of Mars and over the range of energies for the initial particles (7). The first line, "Sputtered O," is the loss of O from Mars due to sputtering calculated in the current work. The next two lines, "exospheric O" and "pickup O^+," are the two other major O loss processes. These values are taken from Luhmann *et al.* (1). The sputtered CO_2 flux is the integrated value calculated by the current model. Since the model assumes that each C lost comes from a CO_2 molecule (assuming that the O escapes on its own), this is just the carbon flux from table 1. The escaped H_2O flux is the flux of water from the other two listed O escape mechanisms as well as sputtering. Again, it is assumed that the necessary H atoms escape for each O. The O escaping as part of the CO_2 is not counted for the water. All of the fluxes are in particles per second.

	Epoch		
	6 EUV (1 Gyr)	3 EUV (2 Gyr)	1 EUV (4.5 Gyr)
Sputtered O:	2.2×10^{28}	1.3×10^{27}	3.5×10^{24}
Exospheric O:	1×10^{26}	5×10^{26}	8×10^{25}
Pickup O^+:	3×10^{27}	4×10^{26}	6×10^{24}
Sputtered CO_2:	6.2×10^{27}	4.9×10^{26}	1.9×10^{24}
Escaped H_2O:	1.4×10^{28}	1.2×10^{27}	8.6×10^{25}

Fig 1. The sputtering loss rates over the history of the Martian atmosphere. The loss rates have been integrated over the planet and (for sputtering) over all incident energies. The actual fluxes were only calculated at 1 Gyr, 2 Gyr and 4.5 Gyr (present). The actual values are listed in table 2. The sputtered CO_2 (d) is based on the escape rate of C and assumes that sufficient O will escape to compensate. The total H_2O line (a) is all the rest of the O since the H is easily lost (12). The O comes primarily from sputtering (c) and exospheric loss (b). The exospheric O is from O_2^+ dissociative recombination. For comparison to the sputtered fluxes calculated in the current work ((c) and (d) for the O and CO_2 respectively) lines (e) and (f), the sputtered fluxes for O and CO_2 from Luhmann *et al.* (1), are also included.

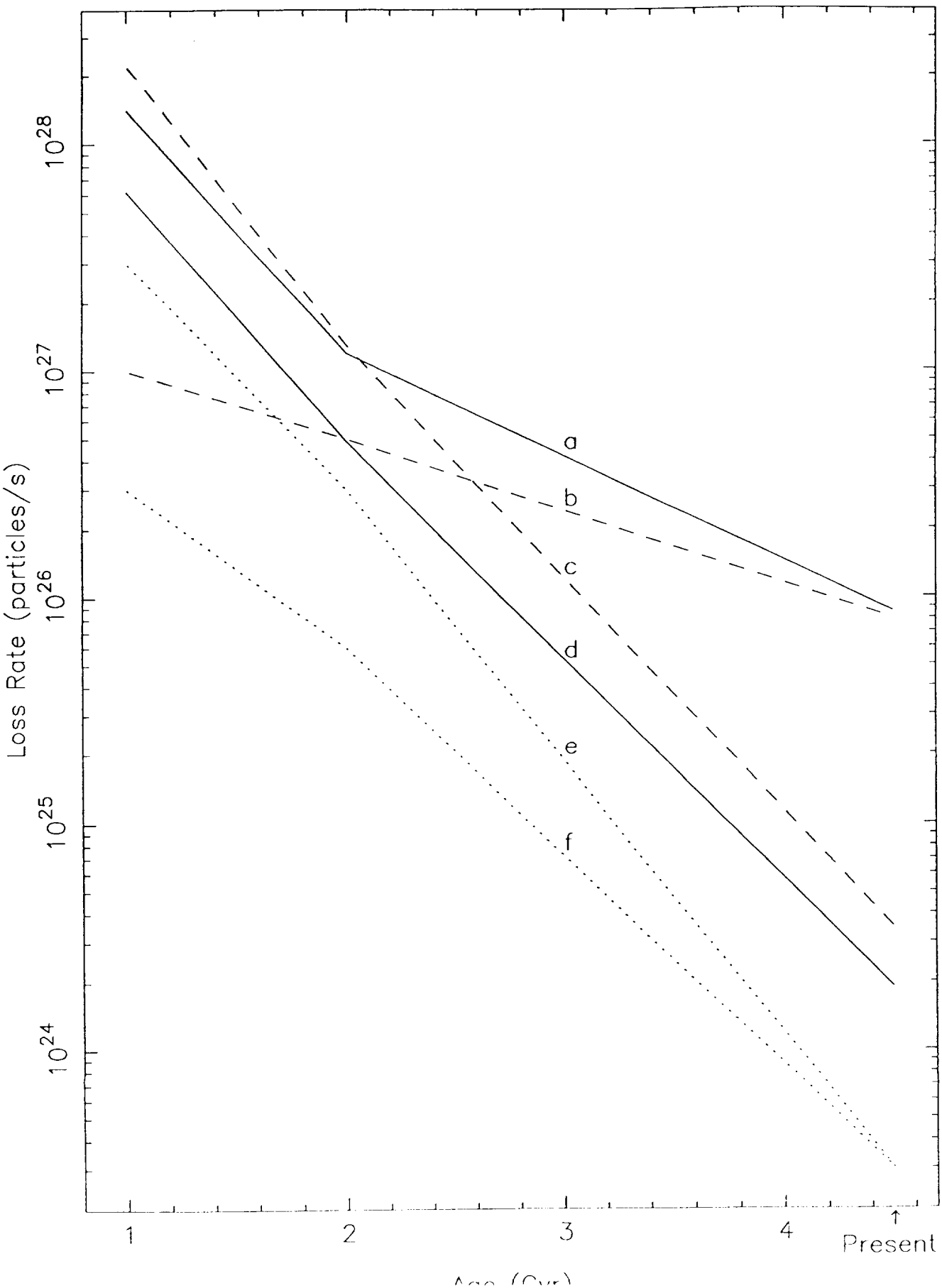
Loss Rate (particles/s)
10^{28}
10^{27}
10^{26}
10^{25}
10^{24}
a
b
c
d
e
f
1
2
3
4
Present
Age (Gyr)